Radio emission from supernovae and gamma-ray bursters and the need for the SKA

Kurt W. Weiler[a] *, Schuyler D. Van Dyk[b], Richard A. Sramek[c], and Nino Panagia[d†]

[a]Naval Research Laboratory, Code 7213, Washington, DC 20375-5320 USA; Kurt.Weiler@nrl.navy.mil

[b]IPAC/Caltech, MS 100-22, Pasadena, CA 91125, USA; vandyk@ipac.caltech.edu

[c]NRAO/VLA, PO Box 0, Socorro, NM 87801 USA; dsramek@nrao.edu

[d]STScI/ESA, 3700 San Martin Dr., Baltimore, MD 21218 USA; panagia@stsci.edu

Study of radio supernovae (SNe) over the past 25 years includes two dozen detected objects and more than 100 upper limits. From this work it is possible to identify classes of radio properties, demonstrate conformance to and deviations from existing models, estimate the density and structure of the circumstellar material and, by inference, the evolution of the presupernova stellar wind, and reveal the last stages of stellar evolution before explosion. It is also possible to detect ionized hydrogen along the line of sight, to demonstrate binary properties of the stellar system, and to show clumpiness of the circumstellar material.

Since 1997 the afterglow of γ-ray bursting sources (GRBs) has occasionally been detected in the radio, as well in other wavelength bands. In particular, the interesting and unusual γ-ray burst GRB 980425, almost certainly related to the radio supernova SN 1998bw, and the more recent SN 2003dh/GRB 030329 are links between the two classes of objects. Analyzing the extensive radio emission data available for SN 1998bw, one can describe its time evolution within the well established framework available for the analysis of radio emission from supernovae. This then allows relatively detailed description of a number of physical properties of the object. The radio emission can best be explained as the interaction of a mildly relativistic ($\Gamma \sim 1.6$) shock with a dense pre-explosion stellar wind-established circumstellar medium that is highly structured both azimuthally, in clumps or filaments, and radially, with observed density enhancements. ¿From this we can support the conclusion that at least some members of the slow-soft class of GRBs are related to type Ib/c SNe and can be attributed to the explosion of a massive star in a dense, highly structured CSM that was presumably established by the pre-explosion stellar system.

However, due to the lack of sensitivity of current radio telescopes, most supernovae cannot be studied if they are more distant than the Virgo Cluster (~ 20 Mpc) or, for exceptionally luminous Type IIn supernovae, beyond ~ 100 Mpc. While the γ-ray bursters are up to 4 orders-of-magnitude more radio luminous, they are also generally much more distant because of their small probability of detection in smaller volumes of space and most are at $z \sim 1$. Those which are radio detected rarely exceed peak flux densities of $\sim 100-300$ μJy. Such low flux densities mean that detailed study of their radio "light curves" and, derived from those light curves, the energetics and dynamics of the explosions and the properties of their progenitors and the circumburst medium is very difficult and severely limited in scope. The increased capability of the SKA to attack these problems will significantly advance the field.

1. INTRODUCTION

Supernovae (SNe) and γ-ray bursters (GRBs) appear to be related since, at least in some cases, they both involve the collapse of a massive stellar progenitor to a neutron star (n*) or black hole

*KWW wishes to thank the Office of Naval Research (ONR) for the 6.1 funding supporting his research.

†Also, Astrophysics Division, Space Science Department of the European Space Agency

(BH) and both involve the release of $\geq 10^{51}$ erg. However, the two areas of study are certainly incompletely merged at the present time and may never completely merge. For example, some types of SNe (e.g., type Ia) have never been detected in the radio and some classes of GRBs (e.g., the "fast-hard" category) have never yet been identified in any other wavelength range and are proposed to have a different origin than the "slow-soft" GRBs for which some afterglows have been detected.

Thus, we have chosen to roughly divide this work on the radio emission into two parts – SN research and GRB research with connections explained as appropriate.

1.1. Supernovae

Supernovae (SNe) play a vital role in galactic evolution through explosive nucleosynthesis and chemical enrichment, through energy input into the interstellar medium, through creation of stellar remnants such as neutron stars, pulsars, and black holes, and by the production of cosmic rays. SNe are also being utilized as powerful cosmological probes, through their intrinsic luminosities. A primary goal of supernova research is an understanding of progenitor stars and explosion mechanisms for the different SN types. Unfortunately, little is left of the progenitor star after explosion, and only the progenitors of three (SNe 1987A, 1978K, and 1993J), out of more than 1500 extragalactic SNe, have been directly identified in pre-explosion images. Without direct information about the progenitors, examination of the environments of SNe can provide useful constraints on the ages and masses of the progenitor stars.

SNe come in three basic types (e.g., [27]): Ia, Ib/c, and II. Both SNe Ia and SNe Ib/c lack hydrogen lines in their optical spectra, whereas SNe II all show hydrogen in their optical spectra with varying strengths and profiles [92]. SNe Ib and SNe Ic subclasses do not show the deep Si II absorption trough near 6150 Å that characterizes SNe Ia, and SNe Ib show moderately strong He I lines, while SNe Ic show no or only weak He I lines.

These spectral differences are theoretically explained by differences in progenitors. SNe Ia are currently thought to arise from the total disruption of white dwarf stars which accrete matter from a binary companion. In contrast, SNe II, SNe Ib, and SNe Ic are likely the explosions of massive stars. SNe II are presumed to result from the core collapse of massive, hydrogen-rich supergiant stars with masses $8 \lesssim M(M_{\odot}) \lesssim 40$. On the other hand, SNe Ib/c are believed to arise from a massive progenitor which has lost all of its hydrogen envelope prior to explosion (e.g., [85]). One candidate progenitor class for SNe Ib/c is exploding Wolf-Rayet stars (which evolve from stars with $M \gtrsim 40\ M_{\odot}$; e.g., [20,53]). An alternative candidate is exploding, relatively less-massive helium stars in interacting binary systems [83,111].

Possible variants of normal SNe II are the "Type IIn," [91] and the "Type IIb" [25], which both show unusual optical characteristics. SNe IIn show the normal broad Balmer line profiles, but with a narrow peak sitting atop a broad base. The narrow component presumably arises from interaction with a dense ($n \gtrsim 10^7$ cm^{-3}) circumstellar medium (CSM) surrounding the SN. SNe IIb look optically like normal SNe II at early times, but evolve to more closely resemble SNe Ib at late times.

1.2. Gamma-ray bursters

Gamma-ray bursts (GRBs) are "mysterious" flashes of high-energy radiation that appear from random directions in space and typically last a few seconds. They were first discovered by U.S. Air Force Vela satellites in the 1960s and, since then, numerous theories of their origin have been proposed. NASA's Compton Gamma-Ray Observatory (CGRO) satellite detected several thousand bursts, with an occurrence rate of approximately one per day. The uniform distribution of the bursts on the sky led theoreticians to initially suggest that their sources were either very near, and thus uniformly distributed around the solar system, in an unexpectedly large halo around the Galaxy, or at cosmological distances – not very restrictive proposals.

Only after the launch of the Italian/Dutch satellite BeppoSAX in 1996 was it possible to couple a quick response pointing system with relatively high precision position sensitive detectors for γ-rays and hard X-rays. This quick response, coupled with high accuracy position information, finally permitted rapid and accurate follow-up observations at other wavelengths with ground- and space-based telescopes, and led to the discovery of long-lived afterglows of the bursts in soft X-rays, visible and infrared light, and radio waves. Although the γ-ray bursts generally last only seconds, their afterglows have, in a few cases, been studied for minutes, hours, days, or even weeks after discovery. These longer wavelength observations have allowed observers to probe the immediate environment of γ-ray burst sources and to assemble clues as to their nature.

The first GRB related optical transient was identified for GRB970228 by Groot et al. [48] with followup by the Hubble Space Telescope (HST) [90]. It showed that the GRB was associated with a faint (thus probably distant) late-type galaxy. A few months later Fruchter, Bergeron and Pian [37] (see also, Pian et al. [81]) imaged the afterglow of GRB970508 with the HST-WFPC2, finding this source to be associated with a late type galaxy at a redshift of $z = 0.835$ and finally demonstrating conclusively that GRBs are at cosmological distances. GRB970508 was also the first GRB to be detected in its radio afterglow [29].

More than a dozen GRBs have now been associated with afterglows in one or more longer wavelength bands. As with the RSNe, we shall concentrate on the GRBs which have been detected in their radio afterglow.

Radio observations are a particularly useful technique for studying GRB afterglows. Frail et al. [32] point out that radio observations are relatively immune to the geometry of the relativistic fireball (presently the preferred model for the GRB phenomenon); the radio afterglow is much more slowly developing than at optical or X-ray wavelengths permitting, within the logistics of discovering, pinpointing, and following up on GRB reports, observation of the critical early phases of the source evolution; and, the observation of interstellar scintillation (ISS), which is only observable at radio wavelengths, provide a possibility for placing observational size limits on the emitting region.

2. RADIO SUPERNOVAE

2.1. Introduction to radio supernovae

A series of papers on radio supernovae (RSNe) has established the radio detection and, in a number of cases, radio evolution for approximately two dozen objects: 3 type Ib supernovae (SNe), 5 type Ic SNe (Because the differences between the SN optical classes are slight – type Ib show strong He I absorption while type Ic show weak He I absorption – and there are no obvious radio differences, we shall often refer to the classes as type Ib/c.), and the rest type II SNe. A much larger list of more than 100 additional SNe have low radio upper limits (See *http://rsd-www.nrl.navy.mil/7213/weiler/kwdata/rsnhead.html*).

In this extensive study of the radio emission from SNe, several effects have been noted:

- type Ia SNe are not radio emitters to the detection limit of the VLA[3]
- type Ib/c SNe are radio luminous with steep spectral indices (generally $\alpha < -1$; $S \propto \nu^{+\alpha}$) and a fast turn-on/turn-off, usually peaking at 6 cm near or before optical maximum.
- type II SNe show a range of radio luminosities with flatter spectral indices (generally $\alpha > -1$) and a relatively slow turn-on/turn-off, usually peaking at 6 cm significantly after optical maximum.

There are a large number of physical properties of SNe which can be determined from radio observations. VLBI imaging shows the symmetry of the blastwave and the local CSM, estimates the speed and deceleration of the SN blastwave propagating outward from the explosion and, with assumptions of symmetry and optical line/radiosphere velocities, allows independent distance estimates to be made (see, e.g., [3,68]).

Measurements of the multi-frequency radio light curves and their evolution with time show

[3]The VLA telescope of the National Radio Astronomy Observatory is operated by Associated Universities, Inc. under a cooperative agreement with the National Science Foundation.

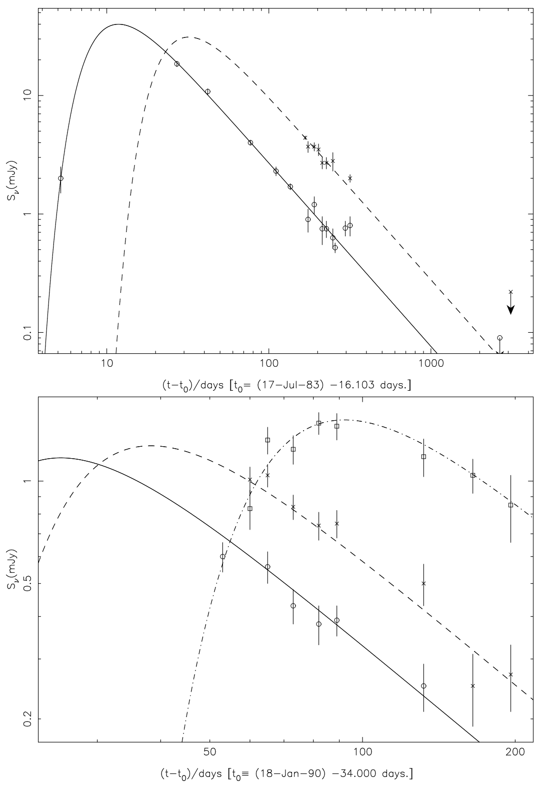

Figure 1. Top (1a): type Ib SN 1983N at 6 cm (4.9 GHz; *open circles, solid line*) and 20 cm (1.5 GHz; *stars, dashed line*). Bottom (1b): type Ic SN 1990B. at 3.6 cm (8.4 GHz; *open circles, solid line*), 6 cm (4.9 GHz; *stars, dashed line*), and 20 cm (1.5 GHz; *open squares, dash-dot line*).

the density and structure of the CSM, evidence for possible binary companions, clumpiness or filamentation in the presupernova wind, mass-loss rates and changes therein for the presupernova stellar system and, through stellar evolution models, estimates of the ZAMS presupernova stellar mass and the stages through which the star passed on its way to explosion.

2.2. Radio supernova models

All known RSNe appear to share common properties of:

- Nonthermal synchrotron emission with high brightness temperature.
- A decrease in absorption with time, resulting in a smooth, rapid turn-on first at shorter wavelengths and later at longer wavelengths.
- A power-law decline of the flux density with time at each wavelength after maximum flux density (optical depth ~ 1) is reached at that wavelength.
- A final, asymptotic approach of spectral index α ($S \propto \nu^{+\alpha}$) to an optically thin, nonthermal, constant negative value [120,121].

The characteristic RSN radio light curves such as those shown in Fig. 1 arise from the competing effects of slowly declining non-thermal radio emission and more rapidly declining thermal or non-thermal absorption yielding a rapid turn-on and slower turn-off of the radio emission at any single frequency. This characteristic light curve shape is also illustrated schematically in Fig. 1 of Weiler et al. [125]. Since absorption processes are greater at lower frequencies, transition from optically thick to optically thin (turn-on) occurs first at higher frequencies and later at lower frequencies. After the radiation is completely optically thin and showing the ongoing decline of the underlying emission process (turn-off), the non-thermal spectrum causes lower frequencies to have higher flux density. These two effects cause the displacement in time and flux density of the light curves at different frequencies also seen in Fig. 1.

Chevalier [14,15] has proposed that the relativistic electrons and enhanced magnetic field necessary for synchrotron emission arise from the SN blastwave interacting with a relatively high density CSM which has been ionized and heated by the initial UV/X-ray flash. This CSM density (ρ), which decreases as an inverse power, s, of the radius, r, from the star, is presumed to have been established by a presupernova stellar wind with mass-loss rate, $\dot{M}$, and velocity, $w_{\rm wind}$, (i.e., $\rho \propto \frac{\dot{M}}{w_{\rm wind}\ r^s}$) from a massive stellar progenitor or companion. For a constant mass-loss rate and constant wind velocity $s = 2$. This ionized CSM is the source of some or all of the initial thermal gas absorption, although Chevalier [16] has proposed that synchrotron self-absorption (SSA) may play a role in some objects.

A rapid rise in the observed radio flux density results from a decrease in these absorption processes as the radio emitting region expands and the absorption processes, either internal or along the line-of-sight, decrease. Weiler et al. [121] have suggested that this CSM can be "clumpy" or "filamentary," leading to a slower radio turn-on, and Montes et al. [71] have proposed the possible presence of a distant ionized medium along the line-of-sight that is sufficiently distant from the explosion that it is unaffected by the blastwave and can cause a spectral turn-over at low radio frequencies. In addition to clumps or filaments, the CSM may be radially structured with significant density irregularities such as rings, disks, shells, or gradients.

2.3. RSN parameterized radio light curves

Weiler et al. [120,121] and Montes et al. [71] adopted a parameterized model which has been updated in Weiler et al. [127] to (Note that for consistency here we use the notation of F_ν(mJy) rather than the S(mJy) more commonly used by radio astronomers.):

$$F_\nu(\mathrm{mJy}) = K_1 \left(\frac{\nu}{5\ \mathrm{GHz}}\right)^{\alpha} \left(\frac{t-t_0}{1\ \mathrm{day}}\right)^{\beta} e^{-\tau_{\mathrm{external}}} \times \left(\frac{1-e^{-\tau_{\mathrm{CSM_{clumps}}}}}{\tau_{\mathrm{CSM_{clumps}}}}\right)\left(\frac{1-e^{-\tau_{\mathrm{internal}}}}{\tau_{\mathrm{internal}}}\right) \quad (1)$$

with

$$\tau_{\mathrm{external}} = \tau_{\mathrm{CSM_{homog}}} + \tau_{\mathrm{distant}}, \quad (2)$$

where

$$\tau_{\mathrm{CSM_{homog}}} = K_2 \left(\frac{\nu}{5\ \mathrm{GHz}}\right)^{-2.1} \left(\frac{t-t_0}{1\ \mathrm{day}}\right)^{\delta} \quad (3)$$

$$\tau_{\mathrm{distant}} = K_4 \left(\frac{\nu}{5\ \mathrm{GHz}}\right)^{-2.1} \quad (4)$$

and

$$\tau_{\mathrm{CSM_{clumps}}} = K_3 \left(\frac{\nu}{5\ \mathrm{GHz}}\right)^{-2.1} \left(\frac{t-t_0}{1\ \mathrm{day}}\right)^{\delta'} \quad (5)$$

with K_1, K_2, K_3, and K_4 determined from fits to the data and corresponding, formally, to the flux density (K_1), homogeneous (K_2, K_4), and clumpy or filamentary (K_3) absorption at 5 GHz one day after the explosion date t_0. The terms $\tau_{\mathrm{CSM_{homog}}}$ and $\tau_{\mathrm{CSM_{clumps}}}$ describe the attenuation of local, homogeneous CSM and clumpy CSM that are near enough to the SN progenitor that they are altered by the rapidly expanding SN blastwave. The $\tau_{\mathrm{CSM_{homog}}}$ absorption is produced by an ionized medium that completely covers the emitting source ("homogeneous external absorption"), and the $(1-e^{-\tau_{\mathrm{CSM_{clumps}}}})\tau_{\mathrm{CSM_{clumps}}}^{-1}$ term describes the attenuation produced by an inhomogeneous medium ("clumpy absorption"; see [75] for a more detailed discussion of attenuation in inhomogeneous media). The τ_{distant} term describes the attenuation produced by a homogeneous medium which completely covers the source but is so far from the SN progenitor that it is not affected by the expanding SN blastwave and is constant in time. All external and clumpy absorbing media are assumed to be purely thermal, singly ionized gas which absorbs via free-free (f-f) transitions with frequency dependence $\nu^{-2.1}$ in the radio. The parameters δ and δ' describe the time dependence of the optical depths for the local homogeneous and clumpy or filamentary media, respectively.

The f-f optical depth outside the emitting region is proportional to the integral of the square of the CSM density over the radius. Since in the simple Chevalier model the CSM density (constant mass-loss rate, constant wind velocity) decreases as r^{-2}, the external optical depth will be proportional to r^{-3}, and since the blastwave radius increases as a power of time, $r \propto t^m$ with $m \leq 1$ (i.e., m = 1 for undecelerated blastwave expansion), it follows that the deceleration parameter, m, is

$$m = -\delta/3. \quad (6)$$

The model by Chevalier [14,15] relates β and δ to the energy spectrum of the relativistic particles γ ($\gamma = 2\alpha - 1$) by $\delta = \alpha - \beta - 3$ so that, for cases where $K_2 = 0$ and δ is, therefore, indeterminate, one can use

$$m = -(\alpha - \beta - 3)/3. \tag{7}$$

Since it is physically realistic and may be needed in some RSNe where radio observations have been obtained at early times and high frequencies, Eq. (1) also includes the possibility for an internal absorption term. This internal absorption (τ_{internal}) term may consist of two parts – synchrotron self-absorption (SSA; $\tau_{\mathrm{internal_{SSA}}}$), and mixed, thermal f-f absorption/non-thermal emission ($\tau_{\mathrm{internal_{ff}}}$).

$$\tau_{\mathrm{internal}} = \tau_{\mathrm{internal_{SSA}}} + \tau_{\mathrm{internal_{ff}}} \tag{8}$$

$$\tau_{\mathrm{internal_{SSA}}} = K_5 \left(\frac{\nu}{5\ \mathrm{GHz}}\right)^{\alpha-2.5} \left(\frac{t-t_0}{1\ \mathrm{day}}\right)^{\delta''} \tag{9}$$

$$\tau_{\mathrm{internal_{ff}}} = K_6 \left(\frac{\nu}{5\ \mathrm{GHz}}\right)^{-2.1} \left(\frac{t-t_0}{1\ \mathrm{day}}\right)^{\delta'''} \tag{10}$$

with K_5 corresponding, formally, to the internal, non-thermal ($\nu^{\alpha-2.5}$) SSA and K_6 corresponding formally to the internal thermal ($\nu^{-2.1}$) free-free absorption mixed with nonthermal emission, at 5 GHz one day after the explosion date t_0. The parameters δ'' and δ''' describe the time dependence of the optical depths for the SSA and f-f internal absorption components, respectively.

2.4. RSN results

The success of the basic parameterization and modeling has been shown in the good correspondence between the model fits and the data for all subtypes of RSNe: e.g., type Ib SN 1983N (Fig. 1a [102]), type Ic SN 1990B (Fig. 1b [112]), and type II SN 1979C (Fig. 2a [73,122,123]) and SN 1980K (Fig. 2b [72,124]). (Note that after day $\sim$ 4000, the evolution of the radio emission from both SN 1979C and SN 1980K deviates from the expected model evolution and that SN 1979C shows a sinusoidal modulation in its flux density prior to day $\sim$4000.)

Thus, the radio emission from SNe appears to be relatively well understood in terms of blastwave interaction with a structured CSM as described by the Chevalier [14,15] model and its extensions by [71,120,121]. For instance, the fact

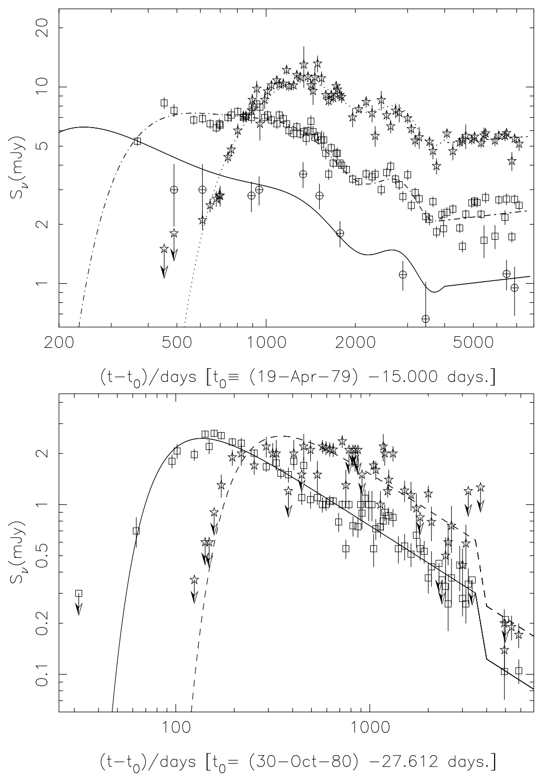

Figure 2. Top (2a): type II SN 1979C at 2 cm (14.9 GHz; *crossed circles, solid line*), 6 cm (4.9 GHz; *open squares, dash-dot line*), and 20 cm (1.5 GHz; *open stars, dotted line*) (Note that the radio flux density increases after day $\sim$ 4000 and has a sinusoidal modulation before day $\sim$ 4000 [73, 122,123].) Bottom (2b): type II SN 1980K at 6 cm (4.9 GHz; *open squares, solid line*), and 20 cm (1.5 GHz; *open stars, dashed line*). (Note a sharp drop in flux density after day $\sim$ 4000 [72].)

that the homogeneous external absorption exponent δ is ~ -3, or somewhat less, for most RSNe is evidence that the absorbing medium is generally an $\rho \propto r^{-2}$ wind as expected from a massive stellar progenitor which explodes in the RSG phase.

Additionally, in their study of the radio emission from SN 1986J, Weiler et al. [121] found that the simple Chevalier [14,15] model could not describe the relatively slow turn-on. They therefore included terms described mathematically by $\tau_{\mathrm{CSM_{clumps}}}$ in Eqs. (1) and (5). This extension greatly improved the quality of the fit and was interpreted by Weiler et al. [121] to represent the presence of filaments or clumps in the CSM. Such a clumpiness in the wind material was again required for modeling the radio data from SN 1988Z [113,130] and SN 1993J [114]. Since that time, evidence for filamentation in the envelopes of SNe has also been found from optical and UV observations (see, e.g., [26,101]).

¿From this modeling there are a number of physical properties of SNe which can be determined from radio observations.

2.4.1. Mass-loss rate from radio absorption

¿From the Chevalier [14,15] model, the turn-on of the radio emission for RSNe provides a measure of the presupernova mass-loss rate to wind velocity ratio ($\dot{M}/w_{\mathrm{wind}}$). Weiler et al. [120] derived this ratio for the case of pure, external absorption by a homogeneous medium. However, Weiler et al. [127] propose several possible origins for absorption and generalize Eq. (16) of Weiler et al. [120] to

$$\frac{\dot{M}(\mathrm{M_\odot\ yr^{-1}})}{(w_{\mathrm{wind}}/10\ \mathrm{km\ s^{-1}})} = 3.0\times10^{-6}\ <\tau_{\mathrm{eff}}^{0.5}> \times m^{-1.5}\left(\frac{v_{\mathrm{i}}}{10^4\ \mathrm{km\ s^{-1}}}\right)^{1.5}\left(\frac{t_{\mathrm{i}}}{45\ \mathrm{days}}\right)^{1.5} \times\left(\frac{t}{t_{\mathrm{i}}}\right)^{1.5m}\left(\frac{T}{10^4\ \mathrm{K}}\right)^{0.68} \quad (11)$$

Since the appearance of optical lines for measuring SN ejecta velocities is often delayed a bit relative to the time of the explosion, they arbitrarily take $t_{\mathrm{i}} = 45$ days. Because observations have shown that, generally, $0.8 \leq m \leq 1.0$ and from Eq. (11) $\dot{M} \propto t_{\mathrm{i}}^{1.5(1-m)}$, the dependence of the calculated mass-loss rate on the date t_{i} of the initial ejecta velocity measurement is weak, $\dot{M} \propto t_{\mathrm{i}}^{<0.3}$, so that the best optical or VLBI velocity measurements available can be used without worrying about the deviation of the exact measurement epoch from the assumed 45 days after explosion. For convenience, and because many SN measurements indicate velocities of $\sim 10,000$ km s^{-1}, one usually assumes $v_{\mathrm{i}} = v_{\mathrm{blastwave}} = 10,000$ km s^{-1} and takes values of $T = 20,000$ K, $w_{\mathrm{wind}} = 10$ km s^{-1} (which is appropriate for a RSG wind), $t = (t_{\mathrm{6cm\ peak}} - t_0)$ days from best fits to the radio data for each RSN, and m from Eq. (6) or (7), as appropriate.

The optical depth term $<\tau_{\mathrm{eff}}^{0.5}>$ used by Weiler et al. [120] is extended by Weiler et al. [127] and they identify at least three possible absorption regimes: 1) absorption by a homogeneous external medium, 2) absorption by a clumpy or filamentary external medium with a statistically large number of clumps, and 3) absorption by a clumpy or filamentary medium with a statistically small number of clumps. These three cases have different formulations for $<\tau_{\mathrm{eff}}^{0.5}>$.

Case 1: Absorption by a homogeneous external medium is the simplest case and has been treated by Weiler et al. [120]. Their result is obtained by substituting

$$<\tau_{\mathrm{eff}}^{0.5}> = \tau_{\mathrm{CSM_{homog}}}^{0.5} \quad (12)$$

which is the homogeneous absorption described in Eq. (3).

Case 2: Absorption by a statistically large number of clumps or filaments is applicable if the number density and the geometric cross section of clumps is large enough so that any line-of-sight from the emitting region intersects many clumps. Then one can use a statistical approach in a scenario that has numerous clumps immersed in a homogeneous medium. For the case of $\delta = \delta'$, it is clear that the fraction of clumpy material remains constant throughout the whole wind established CSM and, therefore, that the radio signal from the SN suffers an absorption $\tau_{\mathrm{CSM_{homog}}}$ from the homogeneous component of the CSM plus an additional absorption, with an even probability distribution between 0 and $\tau_{\mathrm{CSM_{clumps}}}$, from the clumpy or filamentary component of the CSM. In such a case the appropriate average over the possible extremes of the optical depth is taken as

$$<\tau_{\mathrm{eff}}^{0.5}> = 0.67\ [(\tau_{\mathrm{CSM_{homog}}} + \tau_{\mathrm{CSM_{clumps}}})^{1.5} - \tau_{\mathrm{CSM_{homog}}}^{1.5}]\tau_{\mathrm{CSM_{clumps}}}^{-1} \quad (13)$$

with $\tau_{\rm CSM_{homog}}$ and $\tau_{\rm CSM_{clumps}}$ described in Eqs. (3) and (5). Note that in the limit of $\tau_{\rm CSM_{clumps}} \longrightarrow 0$ then $< \tau_{\rm eff}^{0.5} > \longrightarrow \tau_{\rm CSM_{homog}}^{0.5}$ and in the limit of $\tau_{\rm CSM_{homog}} \longrightarrow 0$ then $< \tau_{\rm eff}^{0.5} > \longrightarrow 0.67 \tau_{\rm CSM_{clumps}}^{0.5}$.

Case 3: Absorption by a statistically small number of clumps or filaments is appropriate when the number density of clumps or filaments is small and the probability that the line of sight from a given clump intersects another clump is low. Then both the emission and the absorption will occur effectively within each clump. One still expects a situation with a range of optical depths from zero for clumps on the far side of the blastwave-CSM interaction region to a maximum corresponding to the optical depth through a clump or clumps on the near side of the blastwave-CSM interaction region. One also expects an attenuation of the form $(1 - e^{-\tau_{\rm CSM_{clumps}}}) \tau_{\rm CSM_{clumps}}^{-1}$ but now $\tau_{\rm CSM_{clumps}}$ represents the optical depth along a clump diameter. Moreover, in this case the clumps occupy only a small fraction of the volume and have volume filling factor $\phi \ll 1$. Since the probability that the line of sight from a given clump intersects another clump is low, a condition between the size of a clump, the number density of clumps, and the radial coordinate can be written as

$$\eta \, \pi r^2 \, R \; \approx \; N \; < \; 1 \tag{14}$$

where η is the volume number density of clumps, r is the radius of a clump, R is the distance from the center of the SN to the blastwave-CSM interaction region, and N is the average number of clumps along the line of sight with N appreciably lower than unity by definition. It is easy to verify that there is a relation between the volume filling factor ϕ, r, R and N, of the form

$$\phi = \frac{4}{3} \, \frac{r}{R} \, N. \tag{15}$$

One can then express the effective optical depth $< \tau_{\rm eff}^{0.5} >$ as

$$< \tau_{\rm eff}^{0.5} > = 0.47 \; \tau_{\rm CSM_{clumps}}^{0.5} \phi^{0.5} N^{0.5} \tag{16}$$

where, for initial estimates, one can take $N \sim 0.5$ and a constant ratio $rR^{-1} \sim 0.33$ so that, from Eq. (15), $\phi \sim 0.22$.

While intermediate cases between these three will yield results with larger errors, it is felt, considering other uncertainties in the assumptions, that Eq. (11) with the relations for $< \tau_{\rm eff}^{0.5} >$ given in Eqs. (12), (13), and (16) yield reasonable estimates of the mass-loss rates of the presupernova star. Mass-loss rate estimates from radio absorption obtained in this manner tend to be $\sim 10^{-6}$ M$_\odot$ yr^{-1} for type Ib/c SNe and $\sim 10^{-4} - 10^{-5}$ M$_\odot$ yr^{-1} for type II SNe. Estimates for some of the best studied SNe are listed in Table 1.

2.4.2. Changes in mass-loss rate

A particularly interesting case of mass-loss from an RSN is SN 1993J, where detailed radio observations are available starting only a few days after explosion (Fig. 3a). Van Dyk et al. [114] find evidence for a changing mass-loss rate (Fig. 3b) for the presupernova star which was as high as $\sim 10^{-4}$ M$_\odot$ yr^{-1} approximately 1000 years before explosion and decreased to $\sim 10^{-5}$ M$_\odot$ yr^{-1} just before explosion, resulting in a relatively flat density profile of $\rho \propto r^{-1.5}$.

Fransson and Björgsson [35] have suggested that the observed behavior of the f-f absorption for SN 1993J could alternatively be explained in terms of a systematic decrease of the electron temperature in the circumstellar material as the SN expands. It is not clear, however, what the physical process is which determines why such a cooling might occur efficiently in SN 1993J, but not in SNe such as SN 1979C and SN 1980K where no such behavior is required to explain the observed radio turn-on characteristics. Also, recent X-ray observations with the ROSAT of SN 1993J indicate a non-r^{-2} CSM density surrounding the SN progenitor [55], with a density gradient of $\rho \propto r^{-1.6}$.

Moreover, changes in presupernova mass-loss rates are not unusual. Montes et al. [73] find that type II SN 1979C had a slow increase in its radio light curve after day ~ 4300 (see Fig. 2a) which implied by day 7100 an excess in flux density by a factor of $\sim$1.7 with respect to the standard model, or a density enhancement of $\sim 30\%$ over the expected density at that radius. This may be understood as a change of the average CSM den-

Table 1
Estimated Mass-loss Rates for RSNe[a]

SN	Type	Explosion to 6 cm peak (days)	Flux density at 6 cm peak (mJy)	Peak 6 cm radio luminosity (erg s^{-1} Hz^{-1})	Absorption mass-loss rate ($M_\odot$ yr^{-1})
Type Ib/c					
SN 1983N	Ib	11.6	40.10	1.41×10^{27}	8.74×10^{-7}
SN 1984L	Ib	11.0	4.59	2.57×10^{27}	7.45×10^{-7}
SN 1990B	Ic	37.5	1.26	5.64×10^{26}	2.69×10^{-6}
SN 1994I	Ic	38.1	14.3	1.35×10^{27}	8.80×10^{-6}
SN 1998bw	Ib/c	13.3	37.4	6.70×10^{28}	2.60×10^{-5}
Type II					
SN 1970G	IIL	307.0	21.50	1.40×10^{27}	6.76×10^{-5}
SN 1978K	II	802.0	518.0	1.25×10^{28}	1.52×10^{-4}
SN 1979C	IIL	556.0	7.32	2.55×10^{27}	1.06×10^{-4}
SN 1980K	IIL	134.0	2.45	1.18×10^{26}	1.28×10^{-5}
SN 1981K	II	33.70	5.15	2.14×10^{26}	1.46×10^{-6}
SN 1982aa[b]	II?	476.0	19.10	1.27×10^{29}	1.03×10^{-4}
SN 1986J	IIn	1210.0	135.0	1.97×10^{28}	4.28×10^{-5}
SN 1988Z	IIn	898.0	1.85	2.32×10^{28}	1.14×10^{-4}
SN 1993J	IIb	180.0	95.20	1.50×10^{27}	2.41×10^{-5}

[a]See Sramek et al. [103] for references.
[b]SN 1982aa is not optically identified but behaves like an unusually radio luminous type II.

sity profile from r^{-2}, which was applicable until day ~4300, to an appreciably flatter behavior of $\sim r^{-1.4}$ [73].

On the other hand, type II SN 1980K showed a steep decline in flux density at all wavelengths (see Fig. 2b) by a factor of ~ 2 occurring between day ~3700 and day ~4900 [72]. Such a sharp decline in flux density implies a decrease in $\rho_{\rm CSM}$ by a factor of ~ 1.6 below that expected for a r^{-2} CSM density profile. If one assumes the radio emission arises from a $\sim 10^4$ km s^{-1} blastwave traveling through a CSM established by a ~ 10 km s^{-1} pre-explosion stellar wind, this implies a significant change in the stellar mass-loss rate, for a constant speed wind, at $\sim 12,000$ yr before explosion for both SNe.

2.4.3. Binary systems

In the process of analyzing a full decade of radio measurements from SN 1979C, Weiler et al. [122,123] found evidence for a significant, quasi-periodic, variation in the amplitude of the radio emission at all wavelengths of $\sim 15\%$ with a period of 1575 days or ~ 4.3 years (see Fig. 2a at age < 4000 days). They interpreted the variation as due to a minor ($\sim 8\%$) density modulation, with a period of ~ 4000 years, on the larger, relatively constant presupernova stellar mass-loss rate. Since such a long period is inconsistent with most models for stellar pulsations, they concluded that the modulation may be produced by interaction of a binary companion in an eccentric orbit with the stellar wind from the presupernova star.

This concept was strengthened by more detailed calculations for a binary model from Schwarz and Pringle [93]. Since that time, the presence of binary companions has been suggested for the progenitors of SN 1987A [83], SN 1993J [84] and SN 1994I [77], indicating that binaries may be common in presupernova systems.

2.4.4. Ionized hydrogen along the line-of-sight

A reanalysis of the radio data for SN 1978K from Ryder et al. [88] clearly shows flux density evolution characteristic of normal type II SNe. Additionally, the data indicate the need for a time-independent, free-free absorption component. Montes et al. [71] interpret this con-

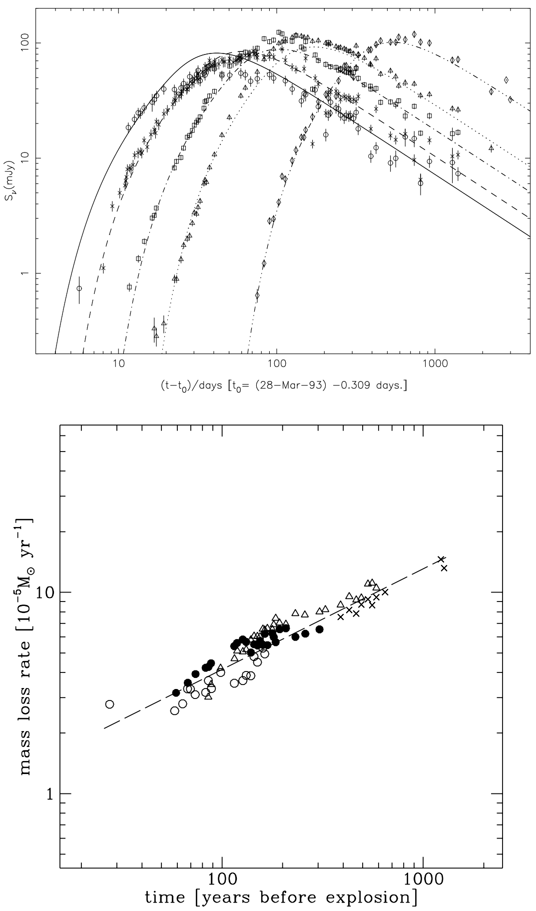

Figure 3. Top (4a): type IIb SN 1993J at 1.3 cm (22.5 GHz; *open circles, solid line*), 2 cm (14.9 GHz; *stars, dashed line*), 3.6 cm (8.4 GHz; *open squares, dash-dot line*), 6 cm (4.9 GHz; *open triangles, dotted line*), and 20 cm (1.5 GHz; *open diamonds, dash-triple dot line*). Bottom (4b): Changing mass-loss rate of the presumed red supergiant progenitor to SN 1993J versus time before the explosion.

stant absorption term as indicative of the presence of HII along the line-of-sight to SN 1978K, perhaps as part of an HII region or a distant circumstellar shell associated with the SN progenitor. SN 1978K had already been noted for its lack of optical emission lines broader than a few thousand km s^{-1} since its discovery in 1990 [88], indeed suggesting the presence of slowly moving circumstellar material.

To determine the nature of this absorbing region, a high-dispersion spectrum of SN 1978K at the wavelength range $6530-6610$ Å was obtained by Chu et al. [18]. The spectrum showed not only the moderately broad Hα emission of the SN ejecta, but also narrow nebular Hα and [N II] emission. The high [N II] 6583/Hα ratio of $0.8-1.3$ region is a stellar ejecta nebula. The expansion velocity and emission measure of the nebula are consistent with those seen in ejecta nebulae of luminous blue variables. Previous low-dispersion spectra have detected a strong [N II] 5755Å line, indicating an electron density of $(3-12)\ \times 10^5$ cm^{-3}. These data suggest that the ejecta nebula detected towards SN 1978K is probably part of a large, dense, structured circumstellar envelope of SN 1978K.

2.4.5. Rapid presupernova stellar evolution

SN radio emission that preserves its spectral index while deviating from the standard model is taken to be evidence for a change of the circumstellar density behavior from the canonical r^{-2} law expected for a presupernova wind with a constant mass-loss rate, $\dot{M}$, and a constant wind velocity, $w_{\rm wind}$. Since the radio luminosity of a SN is proportional to $(\dot{M}/w_{\rm wind})^{(\gamma-7+12m)/4}$ [14] or, equivalently, to the same power of the circumstellar density (since $\rho \propto \frac{\dot{M}}{w_{\rm wind}\ r^2}$), a measure of the deviation from the standard model provides an indication of deviation of the circumstellar density from the r^{-2} law. Monitoring the radio light curves of RSNe also provides a rough estimate of the time scale of deviations in the presupernova stellar wind density. Since the SN blastwave travels through the CSM roughly 1,000 times faster than the stellar wind velocity which established the CSM ($v_{\rm blastwave} \sim 10,000$ km s^{-1} versus $w_{\rm wind} \sim 10$ km s^{-1}), the radio observations are a "time machine" where one year of radio monitoring samples roughly 1000 years of stellar wind mass-loss history.

The best observed example of rapid presupernova evolution is the type II SN 1987A whose proximity makes it easily detectable even at very low radio luminosity. The progenitor to SN 1987A was in a BSG phase at the time of explosion and had ended a RSG phase some ten thousand years earlier. After an initial, very rapidly evolving radio outburst [109] which reached a peak flux density at 6 cm ~ 3 orders-of-magnitude fainter than other known type II RSNe (possibly due to sensitivity limited selection effects), the radio emission declined to a low radio brightness within a year. However, at an age of ~ 3 years the radio emission started increasing again and continues to increase at the present time [1,2,39].

Although its extremely rapid development resulted in the early radio data at higher frequencies being very sparse, the evolution of the initial radio outburst is roughly consistent with the models described above in Eqs. (1)–(10) (i.e., a blastwave expanding into a circumstellar envelope). The density implied by such modeling is appropriate to a presupernova mass-loss rate of a few $\times 10^{-6}$ $M_{\odot}$ yr^{-1} for a wind velocity of $w_{\rm wind} = 1,000$ km s^{-1} (more appropriate to a BSG progenitor), a blastwave velocity of $v_{\rm blastwave} = v_i = 35,000$ km s^{-1}, and a CSM temperature of $T = 20,000$ K.

Because the HST can actually image the denser regions of the CSM around SN 1987A, we know that the current rise in radio flux density is caused by the interaction of the SN blastwave with the diffuse material at the inner edge of the well known inner circumstellar ring [39]. Since the density increases as the SN blastwave interaction region moves deeper into the main body of the optical ring, the flux density is increasing steadily at all wavelengths.

3. RADIO EMISSION FROM GAMMA-RAY BURSTERS

3.1. SN 1998bw/GRB 980425

The probability of an association of the type Ib/c supernova SN 1998bw with the γ-ray burster GRB 980425 provides evidence for another phenomenon generated by SNe – at least some types of GRBs originate in some types of SN explosions. Because SN 1998bw/GRB 980425 is by far the nearest and best studied of the GRBs, it is worthwhile to examine its radio emission in detail before proceeding to the discussion of the radio emission from other GRBs.

3.1.1. Background

While generally accepted that most GRBs are extremely distant and energetic (see, e.g., [46,78]), the discovery of GRB 980425 [100] on 25.90915 April 1998 and its probable association with a bright supernova, SN 1998bw in the relatively nearby spiral galaxy ESO184-G82 at $z = 0.0085$ (distance ~ 40 Mpc for $H_0 = 65$ km s^{-1} Mpc^{-1}) [40,41,43,66,89,108,131], has demonstrated a SN origin for at least some types of GRBs. The estimated explosion date of SN 1998bw is between 21 – 27 April 1998 [89] corresponds rather well with the time of the GRB 980425 outburst. Iwamoto et al. [56] felt that they could restrict the core collapse date for SN 1998bw even more from hydrodynamical modeling of exploding C + O stars and, assuming that the SN 1998bw optical light curve is energized by ^{56}Ni decay as in type Ia SNe, they then placed the coincidence between the core collapse of SN 1998bw to within $+0.7/-2$ days of the outburst detection of GRB 980425.

Classified initially as an SN optical type Ib [89], then type Ic [79], then peculiar type Ic [28,59], then later, at an age of 300 – 400 days, again as a type Ib [80], SN 1998bw presents a number of optical spectral peculiarities that strengthen its probable connection to the γ-ray burst.

3.1.2. Radio emission

The radio emission from SN 1998bw reached an unusually high 6 cm spectral luminosity at peak of $\sim 6.7 \times 10^{28}$ erg s^{-1} Hz^{-1}, i.e., ~ 3 times higher than either of the well studied, very radio luminous type IIn SN 1986J and SN 1988Z, and ~ 40 times higher than the average peak 6 cm spectral luminosity of type Ib/c SNe. It also reached this 6 cm peak rather quickly, only ~ 13 days after explosion.

SN 1998bw was unusual in its radio emission, but not extreme. For example, the time from explosion to peak 6 cm luminosity for both

SN 1987A and SN 1983N was shorter and, in spite of the fact that SN 1998bw has been called "the most luminous radio supernova ever observed," its 6 cm spectral luminosity at peak is exceeded by that of SN 1982aa [132]. However, SN 1998bw is certainly the most radio luminous type Ib/c radio supernova (RSN) observed so far by a factor of ~ 25 and it reached this higher radio luminosity very early.

3.1.3. Expansion velocity

Although unique in neither the speed of radio light curve evolution nor in peak 6 cm radio luminosity, SN 1998bw is certainly unusual in the combination of these two factors – very radio luminous very soon after explosion. Kulkarni et al. [63] have used these observed qualities, together with the lack of ISS at early times, brightness temperature estimates, and physical arguments to conclude that the blastwave from SN 1998bw that gives rise to the radio emission must have been expanding relativistically. On the other hand, Waxman and Loeb [118] argued that a sub-relativistic blastwave can generate the observed radio emission. However, both sets of authors agree that a very high expansion velocity ($\gtrsim 0.3c$) is required for the radio emitting region under a spherical geometry.

Simple arguments confirm this high velocity. To avoid the well known Compton Catastrophe, Kellermann and Pauliny-Toth [60] have shown that the brightness temperature $T_{\rm B} < 10^{12}$ K must hold and Readhead [86] has better defined this limit to $T_{\rm B} < 10^{11.5}$ K. From geometrical arguments, such a limit requires the radiosphere of SN 1998bw to have expanded at an apparent speed $\gtrsim 230,000$ km s^{-1}, at least during the first few days after explosion. Although such a value is only mildly relativistic ($\Gamma \sim 1.6$; $\Gamma = (1 - \frac{v^2}{c^2})^{-\frac{1}{2}}$), it is still unusually high. However, measurements by Gaensler et al. [39] and Manchester et al. [67] have demonstrated that the radio emitting regions of the type II SN 1987A expanded at an *average* speed of $\sim 35,000$ km s^{-1} ($\sim 0.1c$) over the 3 years from February 1987 to mid-1990 so that, in a very low density environment such as one finds around type Ib/c SNe, very high blastwave velocities appear to be possible.

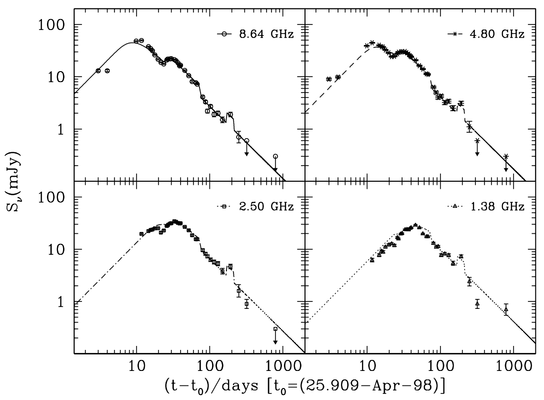

Figure 4. The radio light curves of SN 1998bw at 3.5 cm (8.6 GHz; upper left, *open circles, solid line*), 6.3 cm (4.8 GHz; upper right, *stars, dashed line*), 12 cm (2.5 GHz; lower left, *open squares, dash-dot line*) and 21 cm (1.4 GHz; lower right, *open triangles, dotted line*). (From Weiler et al. [126])

3.1.4. Radio light curves

An obvious comparison of SN 1998bw with other radio supernovae (RSNe) is the evolution of its radio flux density at multiple frequencies and its description by known RSN models. The radio data available from the ATCA (see *http://www.narrabri.atnf.csiro.au/~mwiering/grb/GRB~980425/* are plotted in Fig. 4. SN 1998bw shows an early peak that reaches a maximum as early as day $10 - 12$ at 8.64 GHz, a minimum almost simultaneously for the higher frequencies ($\nu \geq 2.5$ GHz) at day $\sim 20 - 24$, then a secondary, somewhat lower peak after the first dip. An interesting characteristic of this "double humped" structure is that it dies out at lower frequencies and is relatively inconspicuous in the 1.38 GHz radio measurements (see Fig. 4).

Such a double humped structure of the radio light curves can be reproduced by a single energy blastwave encountering differing CSM density regimes as it travels rapidly outward. This is a reasonable assumption because complex density structure in the CSM surrounding SNe, giving rise to structure in the radio light curves, is very well known in such objects as SN 1979C [73,122,123], SN 1980K [72,124] and, particularly, SN 1987A [57].

Weiler et al. [127] pointed out what had not been previously recognized, that there is a sharp drop in the radio emission near day ~ 75 and a single measurement epoch at day 192 that is significantly ($\sim 60\%$) higher at all frequencies than expected from the preceding data on day 149 and the following data on day 249.

Weiler et al. [126–128] were able to explain both of these temporary increases in radio emission by the SN blastwave encountering physically similar shells of enhanced density. The first enhancement or "bump" after the initial outburst peak is estimated to start on day 25 and end on day 75, i.e., having a duration of ~ 50 days and turn-on and turnoff times of about 12 days, where the radio emission (K_1) increased by a factor of 1.6 and absorption (K_3) increased by a factor of 2.0 implying a density enhancement of $\sim 40\%$ for no change in clump size. Exactly the same density enhancement factor and length of enhancement is compatible with the bump observed in the radio emission at day 192 (i.e., the single measurement within the 100 day gap between measurements on day 149 and day 249), even though the logarithmic time scale of Fig. 4 makes the time interval look much shorter. The decreased sampling interval has only one set of measurements altered by the proposed day 192 enhancement, so Weiler et al. [126] could not determine its length more precisely than < 100 days.

Li and Chevalier [65] proposed an initially synchrotron self-absorbed, rapidly expanding blastwave in a $\rho \propto r^{-2}$ circumstellar wind model to describe the radio light curve for SN 1998bw. This is in many ways similar to the Chevalier [16] model for type Ib/c SNe, that also included SSA. To produce the first bump in the radio light curves of SN 1998bw, Li and Chevalier postulated a boost of blastwave energy by a factor of ~ 2.8 on day ~ 22 in the observer's time frame. They did not discuss the second bump.

Modeling of the radio data for SN 1998bw with the well established formalism for RSNe presented above and by [126–128], shows that such an energy boost is not needed. A fast blastwave interacting with a dense, slow, stellar wind-established, ionized CSM, that is modulated in density over time scales similar to those seen for RSNe, can produce a superior fit to the data. No blastwave re-acceleration is required. The parameters of the best fit model are shown as the curves in Fig. 4.

One should note that the fit shown as the curves in Fig. 4 requires no "uniform" absorption ($K_2 = 0$) so all of the free-free (f-f) absorption is due to a clumpy medium as described above. These results, combined with the estimate of a high blastwave velocity, suggest that the CSM around SN 1998bw is highly structured with little, if any, inter-clump gas. The clump filling factor must be high enough to intercept a considerable fraction of the blastwave energy and low enough to let radiation escape from any given clump without being appreciably absorbed by any other clump, which is Case 3 discussed above and by Sramek et al. [103]. The blastwave can then easily move at a speed that is a significant fraction of the speed of light, because it is moving in a very low density medium, but still cause strong energy dissipation and relativistic electron acceleration at the clump surfaces facing the SN explosion center.

3.1.5. Physical parameter estimates

Using the best fit parameters and Eqs. (11) and (16), Weiler et al. [126–128] estimated a mass-loss rate from the pre-explosion star. The proper parameter assumptions are rather uncertain for these enigmatic objects but, for a preliminary estimate, they assumed $t_{\rm i} = 23$ days, $t = (t_{\rm 6cm\ peak} - t_0) = 13.3$ days, $m = -(\alpha - \beta - 3)/3 = 0.78$, $w_{\rm wind} = 10\ \ {\rm km\ s^{-1}}$ (for an assumed RSG progenitor), $v_{\rm i} = v_{\rm blastwave} = 230,000\ \ {\rm km\ s^{-1}}$, and $T = 20,000$ K. They also assumed, because the radio emission implies that the CSM is highly clumped (i.e., $K_2 = 0$), that the CSM volume is only sparsely occupied ($N = 0.5$, $\phi = 0.22$; Case 3). Within these rather uncertain assumptions, Eqs. (11) and (16) yield an estimated mass-loss rate of $\dot{M} \sim 2.6 \times 10^{-5}\ \ {\rm M_{\odot}\ yr^{-1}}$ with density enhancements of $\sim 40\%$ during the two known, extended bump periods.

Assuming that the blastwave is traveling at a constant speed of $\sim 230,000$ km s^{-1} the beginning of the first bump on day 25 implies that it starts at $\sim 5.0 \times 10^{16}$ cm and ends on day 75 at $\sim 1.5 \times 10^{17}$ cm from the star. Correspondingly, if it was established by a 10 km s^{-1} RSG wind, the 50 days of enhanced mass-loss ended $\sim 1,600$ yr and started $\sim 4,700$ yr before the explosion. The earlier high mass-loss rate epoch indicated by the enhanced emission on day 192 in the measurement gap between day 149 and day 249 implies, with the same assumptions, that it occurred in the interval between $\sim 9,400$ yr and $\sim 15,700$ yr before explosion. It is interesting to note that the time between the presumed centers of the first and second increased mass-loss episodes of $\sim 9,400$ yr is comparable to the $\sim 12,000$ yr before explosion at which SN 1979C had a significant mass-loss rate increase [73] and SN 1980K had a significant mass-loss rate decrease [72], thus establishing a possible characteristic time scale of $\sim 10^4$ yr for significant changes in mass-loss rate for pre-explosion massive stars.

3.2. Other gamma-ray bursters
3.2.1. Radio detections

There are relatively few GRBs with detected radio afterglows and only six of these as of 31 December 2001 had sufficient radio light curve information to permit approximate model fits.

GRB 970508 was discovered by the BeppoSax team on 8.904 May 1997 UT [21]. These results showed detection of an afterglow in all wavelength bands including X-ray [82], optical [8], and radio [29]. Metzger et al. [69] found a redshift of $z = 0.835$, which Bloom et al. [6] confirmed for the host galaxy.

The radio data were obtained from the references [10,33,42,94,98]. Representative data for GRB 970508 are plotted, along with curves from the best fit model, in Fig. 5. The parameters of the fit are listed in Weiler et al. [129].

Examination of Fig. 5 shows that the parameterization describes the data well. The 232 GHz upper limits and the 86.7 GHz limits and detections are in rough agreement with the model fitting; the 8.5 GHz and 4.9 GHz measurements are

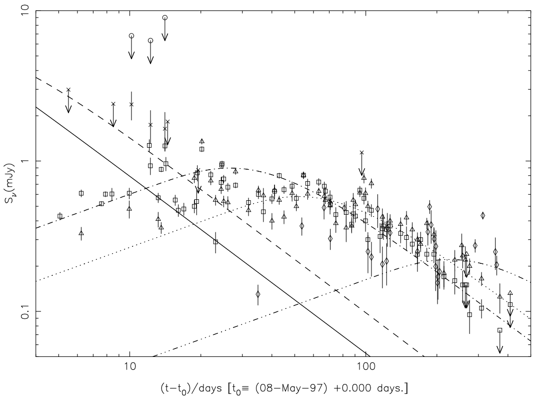

Figure 5. GRB 970508 at radio wavelengths of 1.3 mm (232 GHz; *open circles, solid line*), 3.5 mm (86.7 GHz; *crosses, dashed line*), 3.5 cm (8.5 GHz; *open squares, dash-dot line*), 6 cm (4.9 GHz; *open triangles, dotted line*), and 20 cm (1.5 GHz; *open diamonds, dash-triple dot line*).

described very well, and even the 1.5 GHz data are consistent with the parameterization if significant interstellar scintillation (ISS) is present. Waxman et al. [117] have already ascribed the large fluctuations in the flux density at both 8.5 and 4.9 GHz to ISS, and one expects such ISS to also be present at 1.4 GHz.

GRB 980329 was discovered by the BeppoSax team and also by the BATSE (BATSE Trigger # 6665 [11]) on 29.1559 March 1998 UT [36]. The afterglow was detected in all wavelength bands including X-ray [134], optical [62], and radio [105]. Unfortunately, no redshift has been obtained for the optical afterglow of GRB 980329 or its inferred parent galaxy so that, except for arguments that is quite distant with, perhaps, z $\sim$ 5, no reliable distance estimate is available.

The radio data were obtained from [97,98,106]. Representative data for GRB 980329 are plotted, along with curves from the best fit model, in Fig. 6 and the parameters of the fit are listed in Weiler et al. [129].

Examination of Fig. 6 shows that the parameterization describes the data rather well over the broad parameter space in time and frequency.

Table 2
GRB Radio Afterglows[a]

GRB	Redshift (z)	Spectral Index (α)	Decline Rate (β)	Peak 6 cm Radio Luminosity[b] (erg s^{-1} Hz^{-1})
GRB 970508	0.835	−0.63	−1.18	1.39×10^{31}
GRB 980329	−−	−1.33	−1.09	7.69×10^{30}
GRB 980425	0.0085	−0.71	−1.38	6.70×10^{28}
GRB 980519	−−	−0.75	−2.08	7.52×10^{30}
GRB 991208	0.707	−0.58	−2.27	2.07×10^{31}
GRB 991216	1.020	−0.28	−1.38	1.05×10^{31}
GRB 000301C	2.034	−0.60	$\equiv -1.75$	3.77×10^{31}

[a]See Weiler et al. [129] for more details.
[b]Derived for 6 cm in the rest frame of the observer, not the emitter.

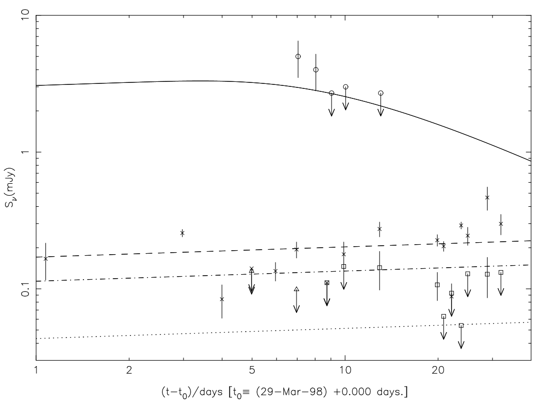

Figure 6. GRB 980329 at radio wavelengths of 0.9 mm (352 GHz; *open circles, solid line*), 3.5 cm (8.5 GHz; *crosses, dashed line*), 6 cm (4.9 GHz; *open squares, dash-dot line*), and 20 cm (1.4 GHz; *open triangles, dotted line*).

The 352 GHz detections and upper limits are in good agreement with the parameterization; the 8.5 GHz and 4.9 GHz measurements are described very well although there may be some ISS present; the 1.4 GHz upper limits are consistent with the parameterization.

Taylor et al. [106] have also modeled the radio data and invoked a somewhat steeper, inverted spectrum with $\alpha = -1.7$ between 4.9 and 8.3 GHz, flattening to $\alpha = -0.8$ between 15 and 90 GHz caused by a SSA component with a turnover frequency near 13 GHz. Extrapolating to higher frequencies, their model predicts a rather low 350 GHz flux density of only ∼1.7 mJy that is incompatible with the JCMT measurements.

Such complexity is not needed, however. The parameterization of [129] shown in Fig. 6 yields a good description of the data and predicts a 350 GHz flux density of ∼3.0 mJy, in much better agreement with the observations.

The model fit of Sramek et al. [103] to the available first 30 days of radio data indicates that GRB 980329 should be detectable with the VLA at centimeter wavelengths, with little decline, for an extended period. Although prediction of exact flux densities at later times is not reliable because the decline phase of the model is not well constrained by the few available data, it is interesting to note that GRB 980329 has apparently been detected by the VLA at 8.46 GHz, 4.86 GHz, and 1.43 GHz for up to 500 days after the outburst [133] but those data have not been made available to us.

GRB 980519 was discovered by the BeppoSax team (BATSE Trigger # 6764) on 19.51410 May 1998 UT [74]. The afterglow was detected in all wavelength bands including X-ray [76], optical [58], and radio [30]. Unfortunately, no redshift has been obtained for the optical afterglow or a

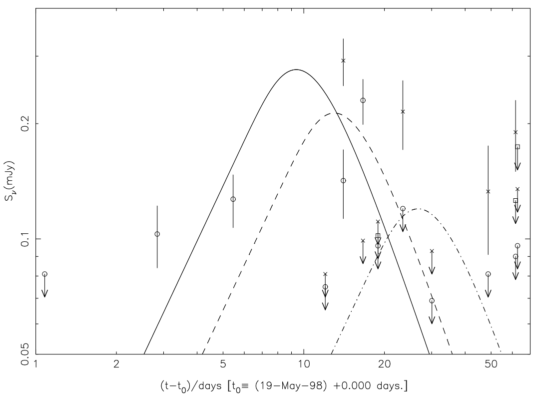

Figure 7. GRB 980519 at radio wavelengths of 3.5 cm (8.5 GHz; *open circles, solid line*), 6 cm (4.9 GHz; *crosses, dashed line*), and 20 cm (1.4 GHz; *open squares, dash-dot line*).

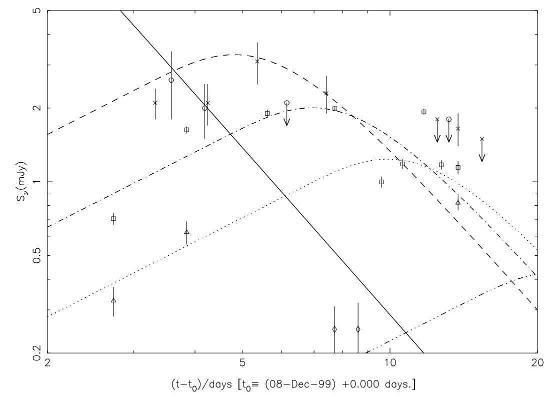

Figure 8. GRB 991208 at radio wavelengths of 1.2 mm (250 GHz; *open circles, solid line*), 2.0 cm (15.0 GHz; *crosses, dashed line*), 3.5 cm (8.5 GHz; *open squares, dash-dot line*), 6 cm (4.9 GHz; *open triangles, dotted line*), and 20 cm (1.4 GHz; *open diamonds, dash-triple dot line*).

host galaxy so that no distance estimate is available.

The radio data were obtained from [33]. Representative data for GRB 980519 are plotted, along with curves from the best fit model, in Fig. 7 and the parameters of the fit are listed in [129].

Examination of Fig. 7 shows that the parameterization describes the data reasonably well, even though the radio data are very limited and of relatively poor quality. For example, the reported detections at 4.9 GHz after day 50 are barely more than 3σ and thus of limited reliability, so that the fit is not well constrained and the significance of their deviation from the best fit curve is unknown. The data at both 8.5 GHz and 4.9 GHz have significant fluctuations yielding detections and 3σ upper limits at relatively small time separations so that GRB 980519 may be undergoing ISS. Only upper limits are available at 1.4 GHz, but they are consistent with the best fit model.

GRB 991208 was discovered by the *Ulysses* and *KONUS* and *NEAR* teams on 08.1923 December 1999 UT [54]. The afterglow was detected in the optical [12] and radio [31] wavelength bands. There does not appear to have been an X-ray detection. Dodonov et al. [23] found a redshift for the parent galaxy of $z = 0.707 \pm 0.002$.

The radio data were obtained from Galama et al. [44]. Representative data for GRB 991208 are plotted, along with curves from the best fit model, in Fig. 8 and the parameters of the fit are listed by Sramek et al. [129].

Examination of Fig. 8 shows that the parameterization describes the data reasonably well. The radio data are quite limited and have relatively large scatter. For example, the reported detection at 15 GHz on day 7.4 is preceded by a 3σ upper limit of comparable magnitude on day 5.4 and followed by an upper limit on day 12.5, so that the reality of the day 7.4 detection must be called into question. In any case, although the fit is not well constrained by the radio data, the model curves describe its evolution reasonably well. The data are too sparse to judge if ISS is present.

GRB 991216 was discovered by BATSE on 16.671544 December 1999 UT (BATSE trigger # 7906) [61]. The afterglow was detected in all wavelength bands including X-ray [104], optical [110], and radio [107]. Vreeswijk et al. [115] suggested a redshift of $z \geq 1.02$ based on the highest redshift of three possible absorption systems seen

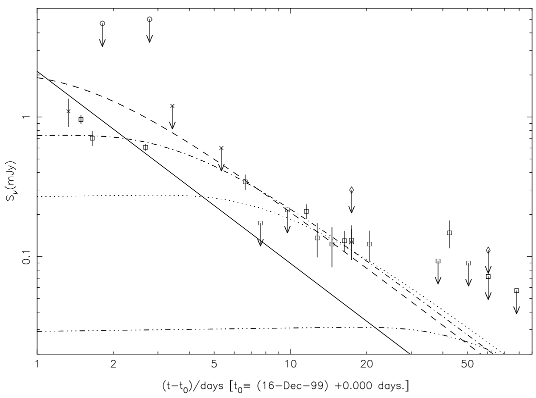

Figure 9. GRB 991216 at radio wavelengths of 0.9 mm (350 GHz; *open circles, solid line*), 2.0 cm (15.0 GHz; *crosses, dashed line*), 3.5 cm (8.5 GHz; *open squares, dash-dot line*), 6 cm (4.9 GHz; *open triangles, dotted line*),and 20 cm (1.4 GHz; *open diamonds, dash-triple dot line*).

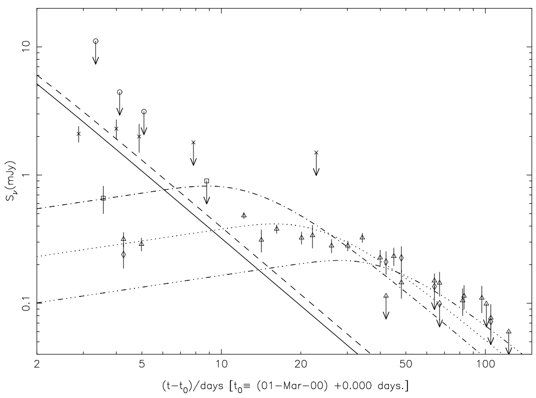

Figure 10. GRB 000301C at radio wavelengths of 0.9 mm (350 GHz; *open circles, solid line*), 1.2 mm (250 GHz; *crosses, dashed line*), 2.0 cm (15.0 GHz; *open squares, dash-dot line*), 3.5 cm (8.5 GHz; *open triangles, dotted line*), and 6.0 cm (4.9 GHz; *open diamonds, dash-triple dot line*).

in the optical afterglow.

The radio data were obtained from Frail et al. [34]. Representative data for GRB 991216 are plotted, along with curves from the best fit model, in Fig. 9.

Examination of Fig. 9 shows that the parameterization fits the data reasonably well, even with the radio data being quite limited and with relatively large scatter. The single detection at 8.5 GHz on day 42.49 surrounded by much lower 3σ upper limits on days 38.28 and 50.51, if correct, is not well described. The data are too sparse to judge if ISS is observed.

GRB 000301C was discovered by the *Ulysses* and *NEAR* teams on 01.4108 March 2000 UT [99]. The afterglow was detected in the optical [38] and radio [5] wavelength bands. There does not appear to have been an X-ray detection. Castro et al. [13] (see also [95]) found a redshift for the parent galaxy of $z = 2.0335 \pm 0.003$.

The radio data were obtained from Berger et al. [4]. Representative data for GRB 000301C are plotted, along with curves from the best fit model, in Fig. 10.

Examination of Fig. 10 shows that the parameterization is successful in that it describes the data rather well over the large frequency and time range. The 350 GHz upper limits and the 250 GHz detections and limits are in rough agreement with the parameterization; the 15 GHz and 8.5 GHz measurements are also consistent with the modeling, although the model drops off a bit faster at late times than the data and the fit would be improved by a somewhat flatter decline rate of $\beta \sim -1.5$. The 1.4 GHz data are generally consistent with the model, although ISS may be present in the first measurement.

3.3. Discussion

Although many useful conclusions can be drawn from the radio light curve parameterizations, one should keep in mind that a more detailed study of radio GRBs will have to take into account several physical effects that are not seen in RSNe, and that have not been included in this brief overview, but need further consideration.

3.3.1. Interstellar Scintillation:

Because their high radio luminosity and low absorption allows detection at great distance and quite early when they are still of very small angular size, GRB radio afterglows appear to be so compact as to exhibit ISS during the first few days or weeks of detectability. This possibility was proposed by Goodman [47] for GRB 970508 based on earlier work by Rickett [87] for pulsars. After consideration of the several regimes of strong, weak, refractive, and diffractive scattering, Goodman [47] concluded that both diffractive and refractive scintillation are possible for radio afterglows and that observation of the effects of scintillation can place limits on their μas (micro-arcsecond) sizes at levels far too small to be resolved with VLBI.

GRB 970508 shows strong flux density fluctuations at both 8.46 and 4.86 GHz until age $\sim$4 weeks after explosion, that Waxman et al. [117] attributed to diffractive scintillation. After $\sim$1 month, they found that the modulation amplitude decreased, which is consistent with the diffractive scintillation being quenched by the increased size of the radio emitting region. They also took this increasing source size to be consistent with, and supportive of, the "fireball" model predictions. From their 4.86 and 8.46 GHz results, Waxman et al. [117,119] concluded that the quenching of diffractive scintillation at $\sim$4 weeks implies a size at that epoch of $\sim 10^{17}$ cm and an expansion speed comparable to that of light.

In contrast to the conclusion of Waxman et al. [117] that GRB 970508 is undergoing strong diffractive scintillation during the first 30 days after explosion, Smirnova and Shishov [96] concluded that the radio afterglow is, in fact, undergoing only weak scintillation at 4.86 and 8.46 GHz at early times with refractive scintillation dominating at 1.43 GHz.

GRB 980329 shows rapid flux density fluctuations at 4.9 and 8.3 GHz that are extinguished by age $\sim$ 3 weeks. Although they did not analyze the scintillation data in detail, Taylor et al. [106] pointed out a similarity to the better studied scintillations of GRB 970508 and suggested that the early-time angular size of GRB 980329 may be even smaller than the ~ 3 μas inferred for GRB 970508 by Goodman [47] and Waxman et al. [117] because GRB980329 is at a lower Galactic latitude, that should more quickly quench ISS.

GRB 980519 shows strong modulation of the flux density at 4.86 and 8.46 GHz during the first $\sim$20 days after the GRB burst, that Frail et al. [33] interpreted as being due to diffractive ISS. They derived a resulting maximum radio source size of < 0.4 μas, an extremely compact object. As was seen for GRB 970508, the 1.4 GHz emission from GRB980519 seems to be suppressed, in this case below their detectability limit because their three measurements at 1.4 GHz are all upper limits. Frail et al. [33] attributed this suppression to SSA with a turn-over frequency between 1.43 and 4.86 GHz.

3.3.2. Cosmological Effects:

Because the GRBs are at cosmological distances ($z \sim 1$), there are two effects that must be taken into account:

- The first is that there is a time dilation that slows the light curve evolution in the observer's frame with respect to the time evolution in the emission frame. This is a straightforward correction and has been elaborated by a number of authors (see, e.g., [19,49,64]). The time dilation results in a true emitted time to 6 cm peak flux density $[(t_{\rm 6cm\ peak} - t_0)_{\rm emit}]$ shorter than that actually observed $[(t_{\rm 6cm\ peak} - t_0)_{\rm obs}]$. The correction takes the form

$$(t_{\rm 6cm\ peak} - t_0)_{\rm emit} = (t_{\rm 6cm\ peak} - t_0)_{\rm obs} \times (1+z)^{-1} \quad (17)$$

  and must be applied to the measured times from explosion to 6 cm peak flux density to obtain true times.

- The second is that there is a correction of the observed flux density, $(F_{\rm 6cm})_{\rm obs}$, owing to the redshift making the observed frequency different from that emitted, $(F_{\rm 6cm})_{\rm emit}$, for sources with non-zero spectral indices. The correction normally takes the form, for $F \propto \nu^{+\alpha}$,

$$(F_{\rm 6cm})_{\rm emit} = (F_{\rm 6cm})_{\rm obs}\ (1+z)^{-\alpha} \quad (18)$$

However, Chevalier and Li [17] have proposed an "equality of peaks" on theoretical grounds so that such a correction may be less important than expected.

3.3.3. Relativistic Effects

Essentially all researchers agree that the GRB phenomenon involves relativistic motion of the emitting region. Whether the motion involves a spherical, relativistic fireball or a directed relativistic jet is probably not of concern from the radio observer's standpoint because the emission from the CSM interaction is probably not highly directed.

For relativistic corrections there are two factors – the Lorentz factor Γ [$\Gamma = (1 - \frac{v^2}{c^2})^{-\frac{1}{2}}$] and, if the motion is directed, the viewing angle θ. If, as expected, the radio emission is not highly directed, then taking $\theta = 0$ leaves only the Lorentz factor Γ to be determined.

The factor Γ is difficult to estimate from observations. Theoretical modeling predicts Γ of several hundred very early in the expansion phase [116] declining to subrelativistic motion after only a few days to a few weeks [22,52].

4. THE NEED FOR THE SKA

4.1. Type Ia SNe

Type Ia SNe have no radio detections, no knowledge of their radio properties and, therefore, little or no knowledge of their CSM environments and the pre-explosion evolution of their progenitors. This is almost certainly due to sensitivity limitations and there have been predictions that radio emission may lie not far below current detection limits for some nearby objects (see, e.g., [7,9,24]. Because of their importance for cosmological studies, increased sensitivity for detection and study of type Ia SNe is of critical importance.

4.2. Type II SNe

Even for Type II SNe, for which we can detect a small fraction of the optically discovered examples, there still exists a large gap in our knowledge between the very faint, somewhat oddball SN 1987A ($\sim 3 \times 10^{23}$ erg s^{-1} Hz^{-1} at 6 cm peak, which could only be detected in the radio because it was extremely nearby in the LMC), and the more "normal" Type II radio SNe, such as SN 1980K ($\sim 1 \times 10^{26}$ erg s^{-1} Hz^{-1}), which can be observed out to roughly the distance of the Virgo Cluster with the VLA sensitivity. The very luminous, but rare RSNe IIn can be observed at larger distances of ~ 100 Mpc.

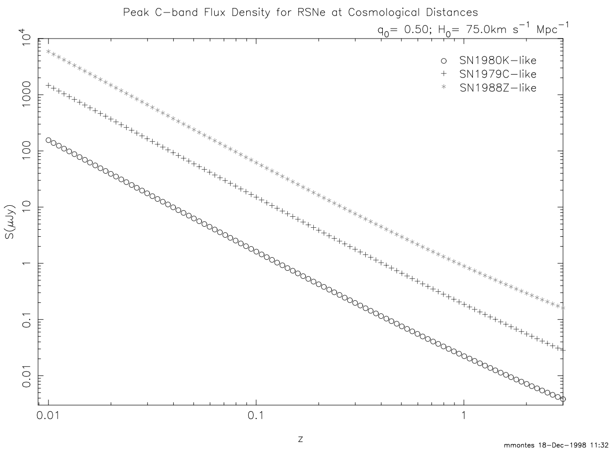

Figure 11. A plot of peak 6 cm (in the observer's frame) flux density for various well-observed RSNe, if they were moved to higher redshift, assuming a Friedmann cosmology ($\Omega_\Lambda = 0$) with $q_0 = 0.50$ and $H_0 = 75$ km s^{-1} Mpc^{-1}. The prototypical RSNe are SN 1980K (*open circles*), SN 1979C (*crosses*), and SN 1988Z (*asterisk*).

However, Fig. 11 illustrates that, with an improved sensitivity level of 1 μJy, one can detect the brightest of RSNe, such as the Type IIn SN 1988Z and SN 1986J, at the cosmologically interesting distance of $z = 1$ and at a sensitivity level of 0.1 μJy one can even study more normal Type II RSNe, such as SNe 1979C and 1980K, at such cosmologically interesting distances.

4.3. GRBs

GRBs have much more powerful radio emission ($\sim 10^{31}$ erg s^{-1} Hz^{-1}), but are generally much more distant so that they are still very weak radio sources and precise measurement of their radio light curves at multiple frequencies is extremely difficult. This is particularly true in the early evolutionary phases which are so important for studying the absorption processes affecting the burst. The early evolution is so rapid that longer integration times to improve sensitivity are not possible. Similarly, following the long term radio evolution after peak flux density in order to describe the structure of the CSM, and its relation to the pre-explosion progenitor system, is excluded because the radio emission drops rapidly below detectability.

4.4. "Dark" bursts

For both SNe and GRBs, improved radio operational capability is needed in order to be able to search for "dark" bursts. For SNe, which are primarily discovered through optical searches, extinction and proximity to the nucleus of a galaxy can lead to "hidden" SNe which are missed in present surveys. For GRBs, the narrowness of the relativistic jet believed to give rise to the γ-ray and X-ray bursts means that most outbursts are missed. The more isotropic radio emission should be detectable for many more objects if radio search capability existed. Thus, for both SNe and GRBs, unbiased radio discovery could provide important new information on the presently poorly known statistics and rates for such objects.

5. CONCLUSIONS AND RECOMMENDATIONS

The current VLA is severely sensitivity limited for SN and GRB studies and the current lack of on-line mapping at the VLA precludes radio searches. Thus, for SN and GRB studies one would like to see:

1. Rms sensitivity of 1 μJy or better in 30 minutes;
2. Resolution ≤ 1 arcsec at 1.4 GHz (preferred also at 327 MHz);
3. Simultaneous, multi-frequency observations;
4. Fast ($\ll 1$ hr) target-of-opportunity (ToO) capability;
5. Real-time, on-line editing, calibration, and mapping; and
6. Nearly circular snapshot beam.

The SKA, and to a lesser extent upgraded VLA, would improve environment/progenitor studies, would increase statistics, and would lead to a better understanding of chemical and dynamical evolution in galaxies. In short, the radio study of SNe and GRBs would be revolutionized.

REFERENCES

1. L. Ball, D. Campbell-Wilson, D.F. Crawford, A.J. Turtle. Astrophys. J. 453 (1995) 864
2. L. Ball, D.F. Crawford, R.W. Hunstead, I. Kalmer, V.J. McIntyre. Astrophys. J. 549 (2001) 599
3. N. Bartel et al. Nature 318 (1985) 25
4. E. Berger et al. Astrophys. J. 545 (2000) 56
5. F. Bertoldi. GCN 580 (2000)
6. J.S. Bloom, S.G. Djorgovski, S.R. Kulkarni, D.A. Frail. Astrophys. J. Lett. 507 (1998) L25
7. F.R. Boffi, D. Branch. Pub. Astron. Soc. Pacific 107 (1995) 347
8. H.E. Bond. IAUC 6654 (1997)
9. D. Branch, M. Livio, L.R. Yungelson, F.R. Boffi, E. Baron. Pub. Astron. Soc. Pacific 107 (1995) 1019
10. M. Bremer, T.P. Kirchbaum, T.J. Galama, A.J. Castro-Tirado, F. Frontera, J. van Paradijs, I.F. Mirabel, E. Costa. Astron. Astrophys. 332 (1998) L13
11. M.S. Briggs, G. Richardson, R.M. Kippen, P.M. Woods. IAUC 6856 (1998)
12. A.J. Castro-Tirado et al. GCN 452 (1999)
13. S.M. Castro, A. Diercks, S.G. Djorgovski, S.R. Kulkarni, T.J. Galama, J.S. Bloom, F.A. Harrison, D.A. Frail. GCN 605 (2000)
14. R.A. Chevalier. Astrophys. J. 259 (1982) 302
15. R.A. Chevalier. Astrophys. J. Lett. 259 (1982) L85
16. R.A. Chevalier. Astrophys. J. 499 (1998) 810
17. R.A. Chevalier, Z.-Y. Li. Astrophys. J. 536 (2000) 195
18. Y.-H. Chu, A. Caulet, M.J. Montes, N. Panagia, S.D. Van Dyk, K.W. Weiler. Astrophys. J. Lett. 512 (1999) L51
19. S.A. Colgate. Astrophys. J. 232 (1979) 404
20. P.S. Conti et al. Astrophys. J. 274 (1983) 302
21. E. Costa et al. IAUC 6649 (1997)

22. Z.G. Dai, Y.F. Huang, T. Lu. Astrophys. J. 520 (1999) 634
23. S.N. Dodonov, V.L. Afanasiev, V.V. Sokolov, A.V. Moiseev, A.J. Castro-Tirado. GCN 465 (1999)
24. C.R. Eck, J.J. Cowan, D.A. Roberts, F.R. Boffi, D. Branch. Astrophys. J. Lett. 451 (1995) L53
25. A.V. Filippenko. Astron. J. 96 (1988) 1941
26. A. Filippenko, T. Matheson, A. Barth. Astron. J. 108 (1994) 222
27. A.V. Filippenko. Ann. Rev. Astron. Astrophys. 35 (1997) 309
28. A. Filippenko. IAUC 6969 (1998)
29. D.A. Frail, S.R. Kulkarni: IAUC 6662 (1997)
30. D.A. Frail, G.B. Taylor, S.R. Kulkarni. GCN 89 (1998)
31. D.A. Frail, S.R. Kulkarni. GCN 451 (1999)
32. D.A. Frail, E. Waxman, S.R. Kulkarni. Astrophys. J. 537 (2000) 191
33. D.A. Frail et al. Astrophys. J. 534 (2000) 559
34. D.A. Frail et al. Astrophys. J. Lett. 538 (2000) L129
35. C. Fransson, C.-I. Björgsson. Astrophys. J. 509 (1998) 861
36. F. Frontera, E. Costa, L. Piro, P. Soffitta, J. in 't Zand, L. Di Ciolo, A. Tesseri. IAUC 6853 (1998)
37. A. Fruchter, L. Bergeron, E. Pian. IAUC 6674 (1997)
38. J.P.U. Fynbo, B.L. Jensen, J. Hjorth, H. Pedersen, J. Gorosabel. GCN 570 (2000)
39. B.M. Gaensler, R.N. Manchester, L. Staveley-Smith, A.K. Tzioumis, J.E. Reynolds, M.J. Kesteven, Astrophys. J. 479 (1997) 845
40. T.J. Galama et al. IAUC 6895 (1998)
41. T.J. Galama et al. Nature 395 (1998) 670
42. T.J. Galama et al. Astrophys. J. Lett. 500 (1998) L101
43. T.J. Galama et al. Astron. Astrophys. Suppl. Ser. 138 (1999) 465
44. T.J. Galama et al. Astrophys. J. Lett. 541 (2000) L45
45. P. Garnavich, R. Kirshner, P. Challis. IAUC 6710 (1997)
46. J. Goodman. Astrophys. J. Lett. 308 (1986) L47
47. J. Goodman. New Astron. 2 (1997) 449
48. P.J. Groot et al. IAUC 6584 (1997)
49. M. Hamuy, M.M. Phillips, L.A. Wells, J. Maza. Pub. Astron. Soc. Pacific 105 (1993) 787
50. G. Hasinger, B. Aschenbach, J. Truemper. Astron. Astrophys. 312 (1996) 9
51. R.M. Hjellming, M.P. Rupen. Nature 375 (1995) 464
52. Y.F. Huang, Z.G. Dai, D.M. Wei, T. Lu. Mon. Not. R. Astron. Soc. 298 (1998) 459
53. R. Humphreys, M. Nichols, P. Massey. Astron. J. 90 (1985) 101
54. K. Hurley, T. Cline. GCN 450 (1999)
55. S. Immler, B. Aschenbach, Q.D. Wang.Astrophys. J. Lett. 561 (2001) L107
56. K. Iwamoto et al. Nature 395 (1998) 672
57. P. Jakobsen et al. Astrophys. J. Lett. 369 (1991) L63
58. A.O. Jaunsen, J. Hjorth, M.I. Andersen, K. Kjernsmo, H. Pedersen, E. Palazzi. GCN 78 (1998)
59. L.E. Kay, J.P. Halpern, K.M. Leighly. IAUC 6969 (1998)
60. K.I. Kellermann, I.I.K. Pauliny-Toth. Astrophys. J. Lett. 155 (1969) L71
61. M.R. Kippen, R.D. Preece, T. Giblin. GCN 463 (1999)
62. S. Klose, H. Meusinger, H. Lehmann. IAUC 6864 (1998)
63. S.R. Kulkarni, J.S. Bloom, D.A. Frail, R. Ekers, M. Wieringa, R. Wark, J.L. Higdon. IAUC 6903 (1998)
64. B. Leibundgut. Astron. Astrophys. 229 (1990) 1
65. Z.-Y. Li, R.A. Chevalier. Astrophys. J. 526 (1999) 716
66. C. Lidman et al. IAUC 6895 (1998)
67. R.N. Manchester, B.M. Gaensler, V.C. Wheaton, L. Staveley-Smith, A.K. Tzioumis, M.J. Kesteven, J.E. Reynolds, N.S. Bizunok. Pub. Astron. Soc. Australia 19 (2002) 207
68. J.M. Marcaide et al. Astrophys. J. Lett. 486 (1997) L31
69. M.R. Metzger, S.G. Djorgovski, C.C. Steidel, S.R. Kulkarni, K.L. Adelberger, D.A. Frail. IAUC 6655 (1997)

70. I.F. Mirabel, L.F. Rodriguez. Nature 371 (1994) 46
71. M.J. Montes, K.W. Weiler, N. Panagia. Astrophys. J. 488 (1997) 792
72. M.J. Montes, S.D. Van Dyk, K.W. Weiler, R.A. Sramek, N. Panagia. Astrophys. J. 506 (1998) 874
73. M.J. Montes, K.W. Weiler, S.D. Van Dyk, R.A. Sramek, N. Panagia, R. Park. Astrophys. J. 532 (2000) 1124
74. J.M. Muller, J. Heise, C. Butler, F. Frontera, L. Di Ciolo, G. Gandolfi, A. Coletta, P. Soffitta. IAUC 6910 (1998)
75. A. Natta, N. Panagia. Astrophys. J. 287 (1984) 228
76. L. Nicastro, L.A. Antonelli, G. Celidonio, M.R. Daniele, C. De Libero, G. Spoliti, L. Piro, E. Pian. IAUC 6912 (1998)
77. K. Nomoto, H. Yamaoka, O.R. Pols, E. van den Heuvel, K. Iwamoto, S. Kumagai, T. Shigeyama. Nature 371 (1994) 227
78. B. Paczynski. Astrophys. J. Lett. 308 (1986) L43
79. F. Patat, A. Piemonte. IAUC 6918 (1998)
80. F. Patat, E. Cappellaro, L. Rizzi, M. Turatto, S. Benetti. IAUC 7215 (1999)
81. E. Pian et al. Astrophys. J. Lett. 492 (1998) L103
82. L. Piro et al. IAUC 6656 (1997)
83. Ph. Podsiadlowski, P.C. Joss, J.J.L. Hsu. Astrophys. J. 391 (1992) 246
84. Ph. Podsiadlowski, J. Hsu, P. Joss, R. Ross. Nature 364 (1993) 509
85. A.C. Porter, A.V. Filippenko. Astron. J. 93 (1987) 1372
86. A.C.S. Readhead. Astrophys. J. 426 (1994) 51
87. B.J. Rickett. Mon. Not. R. Astron. Soc. 150 (1970) 67
88. S. Ryder, L. Staveley-Smith, M. Dopita, R. Petre, E. Colbert, D. Malin, E. Schlegel. Astrophys. J. 417 (1993) 167
89. E.M. Sadler, R.A. Stathakis, B.J. Boyle, R.D. Ekers. IAUC 6901 (1998)
90. K.C. Sahu et al. Astrophys. J. Lett. 489 (1997) L127
91. E.M. Schlegel. Mon. Not. R. Astron. Soc. 244 (1990) 269
92. E.M. Schlegel. Astron. J. 111 (1996) 1660
93. D.H. Schwarz, J.E. Pringle. Mon. Not. R. Astron. Soc. 282 (1996) 1018
94. D.S. Shepherd, D.A. Frail, S.R. Kulkarni, M.R. Metzger. Astrophys. J. 497 (1998) 859
95. A. Smette, A. Fruchter, T. Gull, K. Sahu, H. Ferguson, L. Petro, D. Lindler. GCN 603 (2000)
96. T.V. Smirnova, V.I. Shishov. Astron. Rep. 44 (2000) 421
97. I.A. Smith, R.P.J. Tilanus. GCN 50 (1998)
98. I.A. Smith et al. Astron. Astrophys. 347 (1999) 92
99. D.A. Smith, K. Hurley, T. Cline. GCN 568 (2000)
100. P. Soffitta et al. IAUC 6884 (1998)
101. J. Spyromilio. Mon. Not. R. Astron. Soc. 266 (1994) 61
102. R.A. Sramek, N. Panagia, K.W. Weiler. Astrophys. J. Lett. 285 (1984) L59
103. R.A. Sramek, K.W. Weiler. Supernovae and Gamma-Ray Bursters, ed. K. Weiler (Springer-Verlag LNP 598, Berlin 2003) p. 145
104. T. Takeshima, C. Markwardt, F. Marshall, T. Giblin, R.M. Kippen. GCN 478 (1999)
105. G.B. Taylor, D.A. Frail, S.R. Kulkarni. GCN 40 (1998)
106. G.B. Taylor, D.A. Frail, S.R. Kulkarni, D.S. Shepherd, M. Feroci, F. Frontera. Astrophys. J. Lett. 502 (1998) L115
107. G.B. Taylor, E. Berger. GCN 483 (1999)
108. C. Tinney, R. Stathakis, R. Cannon, T. Galama. IAUC 6896 (1998)
109. A.J. Turtle et al. Nature 327 (1987) 38
110. R. Uglesich, N. Mirabal, J. Halpern, S. Kassin, S. Novati. GCN 472 (1999)
111. A. Uomoto. Astrophys. J. Lett. 310 (1986) L35
112. S.D. Van Dyk, R.A. Sramek, K.W. Weiler, N. Panagia. Astrophys. J. 409 (1993) 162
113. S.D. Van Dyk, R.A. Sramek, K.W. Weiler, N. Panagia. Astrophys. J. Lett. 419 (1993) L69
114. S.D. Van Dyk, K.W. Weiler, R. Sramek, M. Rupen, N. Panagia. Astrophys. J. Lett. 432 (1994) L115
115. P.M. Vreeswijk et al. GCN 496 (1999)
116. E. Waxman. Astrophys. J. Lett. 489 (1997)

L33
117. E. Waxman, S.R. Kulkarni, D.A. Frail. Astrophys. J. 497 (1998) 288
118. E. Waxman, A. Loeb. Astrophys. J. 515 (1999) 721
119. E. Waxman. Supernovae and Gamma-Ray Bursters, ed. K. Weiler (Springer-Verlag LNP 598, Berlin 2003) p. 393
120. K. Weiler, R. Sramek, N. Panagia, J. van der Hulst, M. Salvati. Astrophys. J. 301 (1986) 790
121. K.W. Weiler, N. Panagia, R.A. Sramek. Astrophys. J. 364 (1990) 611
122. K. Weiler, S. Van Dyk, N. Panagia, R. Sramek, J. Discenna. Astrophys. J. 380 (1991) 161
123. K. Weiler, S. Van Dyk, J. Pringle, N. Panagia. Astrophys. J. 399 (1992) 672
124. K. Weiler, S. Van Dyk, N. Panagia, R. Sramek. Astrophys. J. 398 (1992) 248
125. K.W. Weiler, S.D. Van Dyk, M.J. Montes, N. Panagia, R.A. Sramek. Astrophys. J. 500 (1998) 51
126. K.W. Weiler, N. Panagia, M.J. Montes. Astrophys. J. 562 (2001) 670
127. K.W. Weiler, N. Panagia, R.A. Sramek, S.D. Van Dyk, M.J. Montes, C.K. Lacey. The Largest Explosions Since the Big Bang: Supernovae and Gamma-Ray Bursts, eds. M. Livio, N. Panagia, K. Sahu (Cambridge University Press, Cambridge 2000) p. 198
128. K.W. Weiler, N. Panagia, M.J. Montes, R.A. Sramek. Ann. Rev. Astron. Astrophys. 40 (2002) 387
129. K.W. Weiler, N. Panagia, M.J. Montes. Supernovae and Gamma-Ray Bursters, ed. K. Weiler (Springer-Verlag LNP 598, Berlin 2003) p. 367
130. C.L. Williams, N. Panagia, C.K. Lacey, K.W. Weiler, R.A. Sramek, S.D. Van Dyk. Astrophys. J. 581 (2002) 396
131. S.E. Woosley, R.G. Eastman, B.P. Schmidt. Astrophys. J. 516 (1999) 788
132. Q.F. Yin. Astrophys. J. 420 (1994) 152
133. C.H. Young, D.A. Frail, S.R. Kulkarni. Bull. Am. Astron. Soc. 195 (1999) 71.05
134. J. in 't Zand et al. IAUC 6854 (1998)